Enhanced Dispersion and Polarization Interactions Achieved through Dithiophosphate Group Incorporation Yield a Dramatic Binding Affinity Increase for an RNA Aptamer−Thrombin Complex

Martin Egli*,[†,∥,#] and Terry P. Lybrand*,[‡,§,∥,#]

[†]Department of Biochemistry, [‡]Department of Chemistry, [§]Department of Pharmacology, and [∥]Center for Structural Biology, Vanderbilt University, Nashville, Tennessee 37235, United States

S *Supporting Information*

ABSTRACT: Regiospecific replacement of a single phosphate (PO2) by a dithiophosphate (PS2) group in an RNA can dramatically increase its binding affinity for a target protein. Thus, complexes between antithrombin and anti-VEGF RNA aptamers with single dithiophosphate moieties and thrombin and VEGF, respectively, display equilibrium dissociation constants K_D of ca. 1 pM, 1000-fold tighter than the native RNA complexes (ca. 1 nM). Inspection of crystal structures of the native and PS2−RNA aptamer:thrombin complexes reveals an RNA-induced fit in the latter. This leads to a close approach between PS2 and the phenyl ring edge of Phe-232 that is surrounded by pairs of lysines and arginines. To better understand the origins of the tighter binding and individual contributions to the interaction energy, we carried out QM calculations with phosphate− and dithiophosphate− benzene and dimethyl phosphate− and dimethyl dithiophosphate−benzene model systems. These calculations demonstrate that the dithiophosphate−benzene interaction is much stronger than the corresponding interaction with phosphate. QM/MM calculations with the full complexes confirmed this finding and support the hypothesis that the electric field generated by basic residues surrounding Phe-232 is key to the polarization of the PS2 moiety. Thus, disparate polarization and dispersion energies between the PO2 and PS2 complexes contribute critically to the difference in binding affinity. By comparison, easier desolvation of the dithiophosphate group compared to phosphate does not contribute decisively to the observed difference in binding affinity. Favorable polarization and dispersion energies may be a general feature of the dramatic affinity gains seen for complexes between RNAs carrying dithiophosphate groups and their binding proteins.

Energy Decomposition [kcal/mol]		
Contribution	PO2/benzene/PS2	
Electrostatic	-0.9	-2.3
Exchange	0.0	-4.3
Repulsion	0.0	6.9
Polarization	**-0.7**	**-2.0**
Dispersion	**0.0**	**-2.0**
Total Energy	-1.6	-3.7
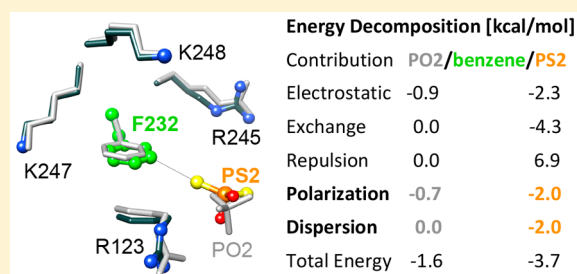
INTRODUCTION

RNA aptamers, short single-stranded ribonucleotide molecules, often exhibit exquisite binding target selectivity for, e.g., proteins or small organic molecules.[1−11] However, weak target binding affinity and poor stability in aqueous solution frequently limit RNA aptamer usage for biomedical applications. A number of straightforward chemical modifications are available to improve chemical stability,[12−15] but to date, there are few simple chemical modifications that lead to significant binding affinity enhancement.

Recently, we reported a simple nucleotide backbone modification in a short RNA aptamer that yielded ∼1000-fold binding affinity enhancement for thrombin.[16] This modification entailed replacement of a single phosphate group with a dithiophosphate (PO_2S_2) group. Our preliminary studies revealed that this extraordinary binding affinity enhancement is achieved only when the dithiophosphate group is substituted at one specific position in the aptamer backbone. Our initial structural analysis, combined with computational studies for simple model systems, provided a plausible explanation for these dramatic results. Here, we report more comprehensive structural and computational studies to obtain a detailed understanding of the sequence-

specific binding affinity enhancement. In agreement with our initial hypothesis, the current studies suggest that the enhanced polarizability of the dithiophosphate group relative to the native phosphate group provides a partial explanation for the binding affinity enhancement. However, our current quantum mechanical calculations for more detailed and realistic model systems, together with coupled quantum mechanical/molecular mechanical (QM/MM) calculations for the full RNA aptamer/thrombin complex, suggest that enhanced dispersion attraction interactions between the dithiophosphate group and specific thrombin residues also make a significant contribution to the increased binding affinity for the dithiophosphate aptamer analogue. The insights we have gained from these structural and computational studies may enable us to make more rational decisions about the possible benefits of dithiophosphate incorporation in RNA aptamer development projects in the future.

■ RESULTS AND DISCUSSION

Overall Structure of the Antithrombin RNA Aptamer Complex with Thrombin. Both the native RNA aptamer and the chemically modified version with the phosphate between U17 and A18 replaced by a dithiophosphate moiety (PS2) bind the target at exosite 2. The overall binding modes are virtually identical, and the modification leaves unaffected both the complex interface area (ca. 420 Å^2) and thrombin conformation (Figure 1).
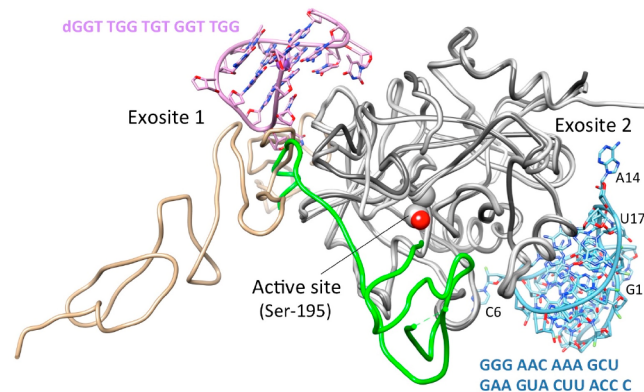
Figure 1. Overlay of the crystal structures of four complexes with human α-thrombin: hirudin (green, PDB ID 4MLF), thrombomodulin (tan, PDB ID 1DX5), RNA aptamer (light blue, PDB ID 3DD2), and DNA aptamer (lilac, PDB ID 4DIH). The active site serine is highlighted, the sequences of the two aptamers are shown adjacent to their structures, and selected RNA residues are labeled. Thrombin molecules in the four complexes are depicted in ribbon mode and colored in different shades of gray.

RNA Conformational Changes. Changes in the conformation of the RNA aptamer bound to thrombin as a consequence of the PS2 moiety in place of the A18 phosphate are mostly limited to residues G16 and U17 and the modified phosphate itself (Table S1). To compare the two RNAs, the nucleic acid portions were extracted from crystal structures of the complexes (PDB ID 3DD2;[17] PDB ID 5DO4[16]) and overlaid with UCSF Chimera,[18] using the match option and the phosphorus atoms of all nucleotides with the exception of G16, U17, and A18. Thus, the phosphate groups of residues A15 and C19 in the native and modified aptamers can be neatly superimposed (Figure 2A). The shifts for phosphorus positions of G16, U17, and A18 are 0.58, 2.57, and 1.58 Å, respectively. The unpaired nucleoside U17 and its 5′-phosphate and 3′-phosphate/PS2 groups exhibit by far the largest change in conformation. Sugar and base undergo a rotation by about 5°, and atoms of the two moieties shift between 1.4 Å (2′-F, ribose C1′) and 2.4 Å (uracil O4). In addition, the 5′-phosphate group of U17 is rotated by ca. 60°. These adjustments are brought about in part by a flip of the G16 ribose from the C2′-endo in the native RNA to the C3′-endo pucker in the PS2−RNA. Moreover, the values of backbone torsion angles ε and ζ of G16 change by 47° (−151 to −104°) and −46° (−82 to −128°), respectively. The most dramatic change concerns the modified phosphate that swings around by ca. 90°, enabled by rotations around torsion angles α and ζ of U17: by −65° from 161° to 96° and by 110° from −60° to 50°, respectively (Figure 2A).

Conformational Changes at the RNA:Thrombin Interface. Replacement of the two nonbridging oxygens of the
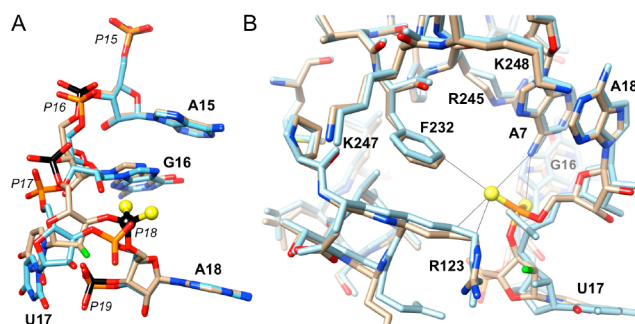
Figure 2. Comparison of the structures of the native and PS2-modified RNA aptamers and aptamer:thrombin complexes. (A) Overlay of the native and PS2−RNA antithrombin aptamers, with carbon atoms colored in light blue and tan, respectively. Only the site of modification and adjacent residues are depicted. Phosphorus atoms in the native and modified backbones are colored in orange and black, respectively, and the PS2 moiety is shown in ball-and-stick mode. (B) Overlay of the native (stick diagram in light blue) and PS2−RNA complexes (colored by atom, with sulfur atoms depicted as yellow spheres). All atoms were included for generating the superimposition. The illustration demonstrates the nearly identical conformations of protein backbone and side chains in the complexes and the local flexing of the RNA at the site of the PS2 modification that results in new H-bonding and hydrophobic interactions by both sulfur atoms (thin solid lines).

phosphate between nucleosides U17 and A18 by sulfur atoms in the antithrombin RNA aptamer results in a remarkable improvement in its affinity for the target by 3 orders of magnitude. The conformational changes seen in the complex between thrombin and modified RNA relative to the native counterpart are limited to the aptamer (Figure 2). Thus, the protein molecules in the two complexes can be superimposed almost perfectly, with side chains of amino acids located at the RNA−thrombin interface displaying very similar conformations. The absence of significant changes in the protein conformation as a consequence of PS2 incorporation is consistent with the record gains in affinity. The RNA-induced fit at the modification site places the SP1 sulfur at 3.7 Å from the phenyl ring of F232 (using the standard chymotrypsinogen-based numbering of bovine thrombin residues[19]) in an edge-on binding mode (Figure 2B). The distance between the corresponding OP1 oxygen in the native structure and the same carbon of the phenyl ring is 7 Å. The closest distance between the OP1 oxygen and the phenyl ring is 5.4 Å. The closer approach between PS2 and the F232 side chain is accompanied by favorable interactions between SP1 and methylene groups of R123 as well as the N6(H)$_2$ amino group of A7. Moreover, the SP2 sulfur is engaged in intra-RNA contacts to the same amino group and C8−H of G16 (Figure 2B). Three hallmarks characterize the PS2-mediated, tighter binding between the RNA aptamer and the protein target: (i) local flexing of the RNA backbone (Supporting Information movie), (ii) hydrophobic interactions enabled by replacing oxygen with sulfur (although both phosphate (PO2) and PS2 carry a negative charge), and (iii) a polarizing electrostatic field generated by basic residues surrounding a hydrophobic core, i.e., R123, R245, K247, and K248, forming a rim around F232 that sits in a shallow depression.

Model System Calculations. We have extended our earlier model system calculations for phosphine oxide and phosphine sulfide with benzene[1] to incorporate a more realistic

representation of the relevant RNA aptamer backbone interactions with the key thrombin phenylalanine residue. In the current study, we performed geometry optimization and energy decomposition analysis calculations for phosphate:benzene and dithiophosphate:benzene complexes. During geometry optimization, the P−O or P−S bond vectors were restrained to geometries observed in the corresponding RNA aptamer:thrombin crystal structures, while all other degrees of freedom were relaxed. The energy decomposition analysis results for these calculations are given in Table 1 and show

Table 1. Model System Energy Decomposition Analysis Results (All Values for Energies in kcal/mol)

contribution	PO_4H_2−benzene	$PO_2S_2H_2$−benzene
electrostatic	−0.9	−2.3
exchange	0.0	−4.3
repulsion	0.0	6.9
polarization	−0.7	−2.0
dispersion	0.0	−2.0
total interaction energy	−1.6	−3.7
static polarizability	∼7.3 Å^3	∼14.1 Å^3

clearly that the dithiophosphate interaction with benzene (i.e., the phenylalanine proxy) is much stronger than the corresponding phosphate:benzene interaction, when each complex is restrained at crystal structure positions. These calculations were repeated using dimethyl phosphate and dimethyl dithiophosphate as the RNA backbone representative, and the results are essentially identical to those obtained for the phosphate and dithiophosphate.

These results are both sensible and anticipated, given the greater polarizability of the dithiophosphate group and the closer approach of the dithiophosphate group to the F232 side chain in the modified aptamer:thrombin crystal structure compared to the wild-type complex. Even when we release all restraints and perform full geometry optimization for each model system, the dithiophosphate complexes still exhibit much more favorable polarization interactions with the aromatic ring. In the unrestrained geometry optimization, the phosphate group does move much closer to the benzene ring, and this results in much stronger electrostatic interactions that offset partially the more favorable polarization and dispersion interactions formed in the dithiophosphate complex. However, this unrestrained optimization yields a more "face-centered" phosphate:benzene complex (i.e., the phosphate group is positioned over the top of the aromatic ring) rather than the "edge-on" complex observed in the crystal structures. This "face-centered" phosphate interaction with the phenylalanine ring is not possible in the aptamer:thrombin complexes, due to considerable steric hindrance posed by residues surrounding F232, as shown in Figure 3.

In our previous study, we proposed that the model system calculations likely *underestimate* the significance of the dithiophosphate:F232 interaction. The F232 side chain is buried in a relatively nonpolar pocket that is surrounded by a collection of basic residues (R123, R245, K247, and K248, Figure 2B). These charged residues generate a strong local electric field, as illustrated by the Coulombic potential surface displayed in Figure 4, and we expect that this strong electric field would enhance the polarization of the dithiophosphate residue as it inserts into the pocket to form the F232 interaction.
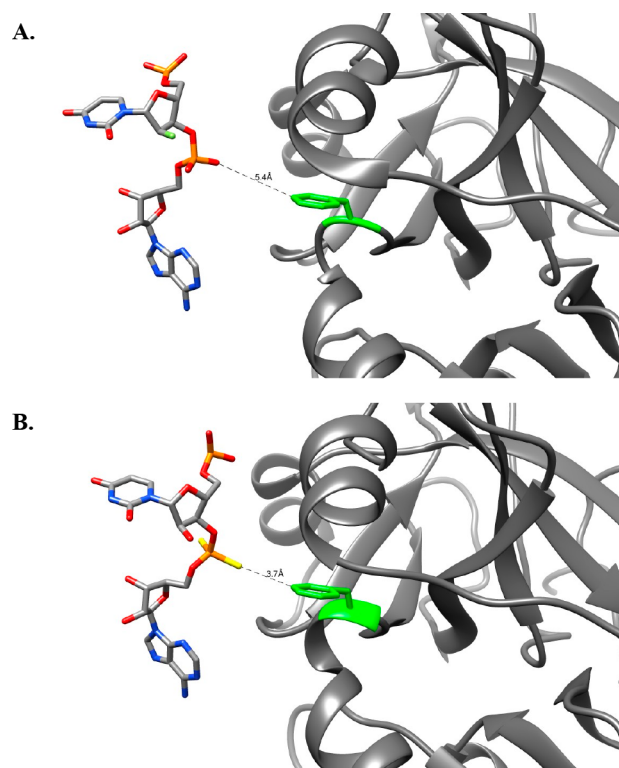
Figure 3. Side view of (A) wild-type aptamer:thrombin complex and (B) dithiophosphate aptamer:thrombin complex. F232 is rendered in green, and only A18 and the preceding U17 aptamer residues are displayed for clarity.
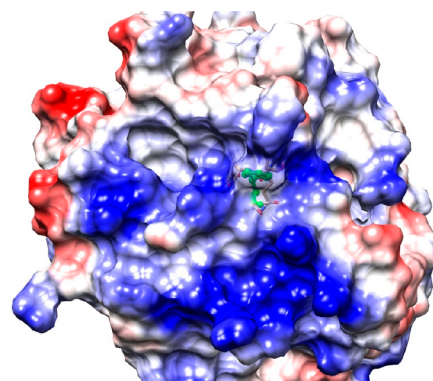
Figure 4. Coulombic potential surface display in the vicinity of the nonpolar pocket where F232 is located (visible at the bottom of the pocket as a green ball-and-stick rendering). The dithiophosphate backbone residue inserts into this pocket in the aptamer:thrombin complex.

Results from QM/MM energy minimization calculations for the full dithiophosphate aptamer:thrombin complex are shown in Table 2 and support our hypothesis that the strong electric field surrounding the dithiophosphate binding pocket does indeed contribute to a strong polarization interaction. Five distinct snapshots for this complex were generated by selecting five distinct configurations from a ∼300 ns molecular dynamics simulation using our preliminary potential function parameters for the dithiophosphate residue. Even though these parameters will need optimization before they are suitable for detailed molecular simulation studies, the aptamer:thrombin complex was stable during the full simulation and the dithiophosphate−

Table 2. Dithiophosphate Aptamer−Thrombin Interaction Energies (kcal/mol) for Five Distinct Complex Configurations

complex	with polarization	without polarization
1)	−51.020	−4.893
2)	−21.845	−5.347
3)	−37.799	−5.551
4)	−0.090	−5.115
5)	−10.459	−5.383
average:	−24.243	−5.258

F232 interaction was well maintained. To compensate for the nonoptimized dithiophosphate potential function parameters, we then subjected each snapshot to full QM/MM geometry optimization, as described in the Experimental Procedures. The sulfur−F232 aromatic ring distance for each optimized snapshot ranged from 3.65 to 3.75 Å, in excellent agreement with the crystal structure. The polarization contribution was estimated by performing the QM/MM energy minimization calculations with electrostatic embedding (i.e., the QM zone is polarized by the electric field due to all atomic partial charges in the MM zone). Then, the interaction energies were recomputed for each optimized complex with mechanical embedding (where the electric field from the MM zone is not included) to approximate the impact of no polarization. The large fluctuations in the computed interaction energy with polarization included are due to dramatically different conformations of charged residues R245, K247, and K248 in each snapshot, which dramatically alters the local electric field in the immediate vicinity of the dithiophosphate binding pocket. By contrast, the calculations performed with mechanical embedding (i.e., the electric field due to neighboring protein residues is neglected) yield consistent results for all five snapshots. The electrostatic embedding approach used in these calculations likely overestimates the polarization contribution due to the electric field generated by the MM zone, and the mechanical embedding calculations are a somewhat simplistic approach to estimate the impact of no polarization. Furthermore, we cannot make any meaningful quantitative estimates of polarization energy contribution using only five aptamer:thrombin complex configurations. However, these results clearly demonstrate that polarization due to charged protein side chains in the vicinity of the binding pocket does have a significant impact on the favorable dithiophosphate:F232 interaction.

To test whether these QM/MM results for the full aptamer:thrombin complex might be artifacts due to limited sampling afforded by the geometry optimization calculations, we then took all five optimized dithiophosphate aptamer complexes, replaced the dithiophosphate group with a phosphate, and performed full geometry optimization with the same protocol and basis set. While these minimization calculations do not fully recover the original wild-type complex configuration observed in the wild-type aptamer:thrombin crystal structure, in all five complexes, we observe that the phosphate−F232 distance increases consistently to ∼4.2 Å. Combined, these results for the wild-type and dithiophosphate aptamer complexes strongly suggest that the intrinsic dithiophosphate:F232 aromatic ring interactions are notably stronger than the corresponding phosphate:F232 interactions.

Since we do have well optimized parameters for a standard nucleic acid phosphoribose backbone, we next took these five newly optimized phosphate aptamer:thrombin configurations and performed classical MD simulations for 300−500 ns each. In each trajectory, the phosphate−F232 distance increased rapidly to ∼5.3 ± 0.3 Å and maintained this contact distance for the duration of each trajectory. We also observe a gradual transition of the backbone torsion angles ε and ζ toward canonical values, although we did not observe a full conformational transition during these relatively short MD simulations. Observation of a complete transition of these torsion angles to canonical values is unlikely unless the aptamer is dissociated from the thrombin complex.

While the QM calculations for the model system and the QM/MM results for the full aptamer:thrombin complexes strongly suggest that the dramatically enhanced binding free energy observed for the dithiophosphate aptamer is due to more favorable polarization and dispersion interactions compared to the wild-type aptamer, there may be some contribution from differential desolvation energies as well. A phosphate group is obviously more polar than the corresponding dithiophosphate, although the dithiophosphate group still carries a formal negative charge, so the polarity difference is not as large as might be anticipated. We do expect a larger energy "penalty" to desolvate the phosphate group during complex formation, and our QM solvation free energy calculations support this assumption, as $\Delta\Delta G_{SOLVATION}$ is predicted to favor dimethyl phosphate over dimethyl dithiophosphate by as much as 4−5 kcal/mol, depending on the level of QM theory and basis set used. Crystal structures of PS2-modified RNA duplexes at atomic resolution reveal that water molecules are located at ca. 3.5 Å from sulfur atoms compared to H-bonds with lengths of ca. 2.8 Å for water around phosphate oxygens.[20] The longer distances in the case of PS2···water interactions are not simply a consequence of the increased van der Waals radius of S relative to O (1.8 and 1.52 Å, respectively) but suggest weakened H-bonds with the former. However, experimental data for the full aptamers suggest that relative desolvation energies for phosphate versus dithiophosphate aptamer probably do NOT make a significant contribution to the overall $\Delta\Delta G_{BINDING}$.

As noted above, we observe a dramatic increase in binding affinity only when the dithiophophate substitution is made at aptamer position A18. However, crystal structures for both the wild-type aptamer:thrombin complex (PDB ID: 3DD2) and our A18-modified aptamer complex (PDB ID: 5DO4) show clearly that multiple phosphate groups are buried in the interface surface. Each of these buried phosphate groups has complete or substantial desolvation upon complex formation, yet we observe no statistically significant change in binding free energy when a dithiophosphate group is substituted at any of these other aptamer backbone positions. These experimental observations strongly suggest that desolvation energy differences for a phosphate versus a dithiophosphate group do not make a significant contribution to the large binding free energy change we measure for the A18-modified aptamer.

There are experimental observations that document the increased hydrophobicity of dithiophosphate-modified RNA compared to the native species, but the effects are generally rather subtle. One of these is the longer retention time of modified RNAs on reversed-phase HPLC columns. PS2 modification also results in slight losses in thermodynamic stability of duplexes compared to the native counterparts.[16,21] However, the reduction in melting temperatures of typically

less than 1 °C per PS2 moiety can be offset by combined PS2/2'-OMe or PS2/2'-F modification.

There is one additional, striking experimental observation that argues against the hypothesis that a significant desolvation difference or hydrophobic effect is at the heart of the record improvements in affinity seen with dithiophosphate-modified RNA aptamers for their protein targets compared to the natural counterparts. The equilibrium dissociation constant K_d of the complex between the antithrombin RNA aptamer with monothiophosphate (Rp-/Sp-PSO) and thrombin is more than 300-fold lower than that for the complex with the dithiophosphate aptamer.[16] Even more remarkable, the difference in K_d for the PSO and PS2 anti-VEGF aptamer complexes with VEGF is more than 10,000-fold in favor of the latter.[16] If hydrophobicity differences between PO2, PSO, and PS2 were the driving force of the observed affinity increases seen with PS2-modified aptamers, one might expect the gains measured for PS2- relative to PSO- and PO2-aptamers to be approximately additive. That is clearly not the case, providing further evidence that differences in hydration and desolvation energies between PS2 and PO2 do not play a decisive role in the affinity increases seen with PS2-modified RNA aptamers. The negative charge of the dithiophosphate group undoubtedly accounts for the much stronger interaction energy of the PS2−aromatic contacts seen here compared to those computed for cysteine− or methionine−aromatic configurations using a H_2S−benzene model system.[22]

We observe changes in the local aptamer backbone conformation at the dithiophosphate residue which facilitate a closer approach of a sulfur atom to the F232 ring. However, these altered backbone torsion angles are not an intrinsic attribute of a dithiophosphate residue. Previous crystal structures with dithiophosphate groups inserted into RNA oligonucleotides exhibit normal canonical backbone torsion angles,[20] so the closer approach of the dithiophosphate residue to F232 in the aptamer:thrombin complex is not due to different backbone conformational preferences but rather an induced fit due to the more favorable dithiophosphate:aromatic ring interaction.

■ CONCLUSIONS

The crystal structures reveal that both the wild-type aptamer and dithiophosphate-modified aptamer complexes with thrombin are strikingly similar. The only notable differences in the two structures are changes in the ribonucleotide backbone angles ε and ζ for G16 and a pseudorotation of the G16 sugar ring from the C2'-endo to the C3'-endo conformation for the dithiophosphate aptamer complex. These local conformational changes enable a sulfur atom of the dithiophosphate group to make a close approach to F232, as shown in Figure 2B. Our model system calculations reveal that this close sulfur−aromatic ring contact leads to a significant increase in favorable dispersion and polarization interactions compared to the native phosphate complex. This result is sensible, given the much larger polarizability of the dithiophosphate group compared to phosphate. The enhanced polarizability of the dithiophosphate group should be even more significant in the thrombin complex, since a cluster of basic residues surrounds the sulfur:F232 interaction site. These residues generate a significant electric field, as displayed qualitatively by the Coulombic potential surface shown in Figure 4. This prominent electric field should polarize the dithiophosphate sulfur atom, leading to an enhanced

interaction with F232, and our coupled QM/MM calculations for the full aptamer complexes support this hypothesis.

It seems quite plausible that the dramatic gains in binding affinity triggered by dithiophosphate modification seen in an RNA aptamer−VEGF complex,[16] as well as other oligonucleotide−protein complexes, might be rationalized in a similar fashion. However, to date, there are relatively few cases of oligonucleotide−protein binding enhancement due to selective PS2 incorporation where we have both detailed thermodynamic measurements AND high-resolution structural data. Figure 5 displays a few relevant examples: (A) Ago2 protein complexed with siRNA sense strand (PDB ID: 4W5T),[24] (B) MS2 phage coat protein with an RNA hairpin (PDB ID:
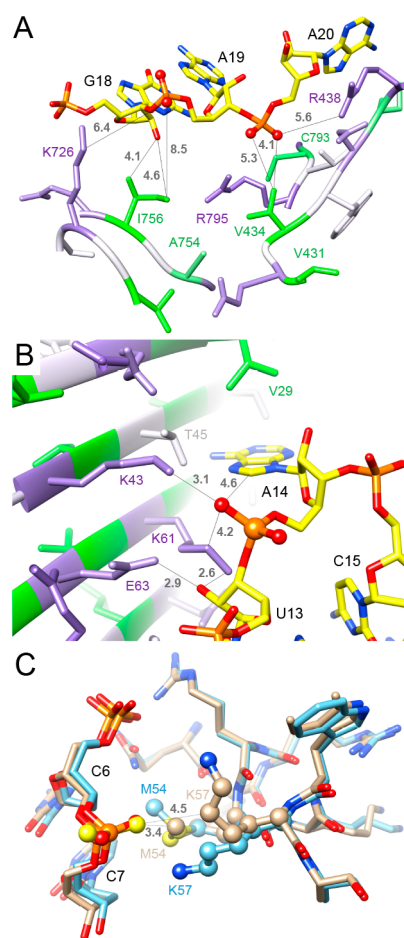
Figure 5. Environments of PO2 groups (highlighted in ball-and-stick mode) for which replacement by PS2 triggers variable gains in binding affinity. (A) siRNA sense strand 3'-penultimate phosphate (A20) and 5'-adjacent one (A19) lodged across residues from the Ago2 PIWI and MID domains based on the crystal structure of the complex with duplex RNA[24] (PDB ID 4W5T): ca. 50,000-fold improvement in K_D from 0.6 μM to 12.4 pM upon substitution of both PO2s by PS2.[20] (B) MS2 phage coat protein interacting with RNA hairpin at A14: ca. 70-fold improvement in K_D from 1.54 nM to 21.8 pM upon substitution of PO2 by PS2.[23] (C) Comparison between native (light blue carbon atoms) and PS2-modified (at C7; tan carbon atoms) DNA operators bound to Antennapedia homeodomain protein[25] (PDB IDs 4XID and 4XIC, respectively): ca. 4-fold improvement in K_D from 11 nM to 2.9 nM upon substitution of PO2 by PS2. Protein residues in the top two panels are colored according to hydrophobicity potential: purple lowest, 0 white, and green highest. All distances are in Å.

1ZDH; 1ZDI),[23] and (C) Antennapedia homeodomain protein bound to native and PS2-modified duplex DNA (PDB ID: 4XIC; 4XID).[25] Analysis of these complexes and comparison with the RNA aptamer:thrombin complex reported here reveal a number of common features.

Perhaps most strikingly, the observed or presumed dithiophosphate binding site on the target protein is in all cases composed almost exclusively of nonpolar residues (Ile, Leu, Met, etc.), and this nonpolar pocket is surrounded by small clusters of Arg and Lys residues. It also appears that dithiophosphate incorporation is more likely to yield meaningful binding enhancements when there is reasonable backbone flexibility at the PS2 substitution site, thus facilitating conformational rearrangements that would enable close contact of the PS2 group with the nonpolar pocket on the target protein.

For example, in the Ago2:RNA complex, substitution of PS2 groups at the penultimate and adjacent phosphate positions (A20 and A19, respectively, Figure 5A) of the siRNA sense strand yields ∼50,000× increased binding affinity relative to the native RNA,[20] and these two PS2 residues are in close proximity to the presumed nonpolar binding pockets on Ago2. The relative flexibility of the RNA backbone at the oligonucleotide terminus should facilitate conformational rearrangement that enables direct interaction of both PS2 groups with the protein, just as we observe in the RNA aptamer:thrombin complex.

The MS2 phage coat protein complex with an RNA hairpin also exhibits a small, nonpolar binding pocket surrounded by basic residues and in close proximity to the PS2 substitution site (Figure 5B). However, the PS2 substitution site is located near the tip of the RNA hairpin, and the backbone is more conformationally restricted in this region. This fact may help explain the modest binding affinity enhancement (∼70×) observed in this complex,[23] as the crystal structures suggest that PS2 insertion into the binding pocket is not as optimal as the interactions observed for the aptamer:thrombin complex.

Finally, the DNA complex with Antennapedia homeodomain protein also reveals a similar nonpolar binding pocket surrounded by basic residues, but in this case, the DNA backbone rigidity appears to limit the ability of the PS2 group to insert fully into the nonpolar pocket (Figure 5C), and the observed binding enhancement is only 4× relative to native DNA.[25] Dithiophosphate substitution in DNA generally does not produce as impressive binding affinity increases as are often observed for RNA. This trend might be due in part to the greater backbone rigidity of DNA and concomitant reduction in tertiary structure complexity compared to RNA, which may limit the ability of DNA oligomers to adopt conformations that enable optimal dithiophosphate interactions with target proteins.

While the available experimental data for the RNA aptamer:VEGF-165 complex strongly suggest a similar scenario,[16] the lack of high-resolution structures for the isolated aptamer, the apo-VEGF-165 protein, or the aptamer:VEGF complex makes it impossible to confirm these proposed interactions at present.

The striking similarities of the dithiophosphate binding site in each protein complex discussed here suggest that our calculations for the aptamer:thrombin complex provide relevant insight for all of these cases. For example, it is highly probable that favorable dispersion interactions due to dithiophosphate substitution make a significant contribution

to the improved binding affinities observed for each complex. Likewise, the small cluster of basic residues that surround the nonpolar pocket in each target protein should polarize the dithiophosphate group, just as we observe for the aptamer:-thrombin complex. Unlike the thrombin complex, none of these other nonpolar binding pockets contain an aromatic residue. However, previous experimental measurements and calculations show that the nonpolar residues present in these binding pockets (e.g., isoleucine, leucine, methionine) are nearly as polarizable as aromatic residues like phenylalanine.[26−29] Therefore, it is perhaps reasonable to expect favorable polarization contributions from dithiophosphate substitution in each case as well. The sulfur−sulfur interaction observed between dithiophosphate and methionine in the DNA−Antennapedia protein complex (Figure 5C) is well documented in many contexts, and previous calculations confirm significant favorable dispersion and polarization contributions for this interaction.[30] In summary, these analyses suggest that our results for the RNA aptamer:thrombin complex are not unique to that system but rather likely applicable to a much wider range of protein complexes with dithiophosphate-modified oligonucleotides.

A more detailed understanding of the mechanism by which dithiophosphate substitution yields RNA aptamers with greatly enhanced target binding affinities may help us make more rational design decisions for dithiophosphate incorporation in future RNA aptamer development projects, and the results we report here should provide useful insight.

■ EXPERIMENTAL PROCEDURES

All geometry optimization calculations for the model systems were performed at the MP2 level of theory with the aug-cc-pVDZ basis set. Final energies and static polarizability for all geometry-optimized molecules and complexes were computed at the CCSD(T) level of theory with the aug-cc-pVTZ basis set. Local minima were confirmed via frequency calculations, and static polarizability was calculated as the mean of the trace of the polarizability tensor. All geometry optimization and energy calculations were performed with the Gaussian 09 package.[31] Energy decomposition analysis was performed using the LMOEDA method,[32] as implemented in the GAMESS-US package.[33] Solvation free energy calculations for dimethyl phosphate and dimethyl dithiophosphate were performed at the CCSD(T) level with the aug-cc-pVTZ basis set using the polarizable continuum model method (PCM)[34] with the SMD model developed by Marenich et al.[35]

Energy minimization calculations for the full aptamer−thrombin complexes were performed using coupled QM/MM calculations with the AMBER14[36] and Gaussian 09[31] packages. The AMBER ff14 potential function[37] was used for the molecular mechanics calculations (i.e., the "MM" zone) along with the SPC/E water model,[38] Joung/Cheatham parameters for monovalent cations with SPC/E water,[39] and Li/Song/Merz 12−6−4 parameters for divalent cations with SPC/E water.[40] The phosphate or dithiophosphate group for nucleotide A18 of the aptamer and the F232 side chain were treated quantum mechanically (i.e., the "QM" zone). The QM zone boundaries were defined to dissect carbon−carbon and carbon−oxygen single bonds, and the linked-atom method was used to treat the QM/MM boundary. The quantum mechanics zone was computed at the MP2 level of theory with a 6-311++G(2d,2p) basis set. All minimization calculations were run until the RMS gradient was less than 0.05 kcal/mol-Å.

Classical MD simulations were performed using the PMEMD AMBER module. Aptamer:thrombin complexes were solvated in a truncated octahedron box with a 14 Å buffer zone between any complex atom and the closest box wall. All starting complexes were subjected to a three-step minimization procedure. First, complex

atoms were relaxed for 10,000 steps of conjugate gradient minimization while water molecules and counterions were restrained at starting positions. Next, all solvent and counterions were relaxed for 10,000 steps while complex atoms were restrained. Finally, all restraints were removed and the entire system was minimized for 10,000 additional steps. Each minimized complex was then heated gradually from 0 to 300 K during a 50 ps canonical ensemble (NVT) MD simulation, followed by a 50 ps simulation in the NPT ensemble. Production MD simulations were then run with a 1.5 fs time step for 300−500 ns. Energy and force calculations were performed using minimal image periodic boundary conditions, a 12 Å nonbonded cutoff for real space interactions, a homogeneity assumption to approximate the contributions of long-range Lennard-Jones forces to the virial tensor, and staggered particle-mesh Ewald for long-range electrostatics correction.[41] A Langevin thermostat with a collision frequency of 3 ps^{-1} was used to maintain the system temperature.[42] All bonds containing hydrogen were constrained using the SHAKE algorithm,[43] and the SETTLE method was used to maintain rigid water geometry.[44]

Preliminary potential function parameters for the dithiophosphate group nonbonded interactions were developed using existing sulfur van der Waals parameters in the AMBER ff14 force field. Partial charges for the dithiophosphate group were computed using the RESP program and protocol.[45] Parameters for bond, bond angle, and torsion angles were extrapolated from corresponding parameters for a nucleotide phosphate. While these preliminary parameters reproduce dithiophosphate structures reasonably well, additional optimization will be needed before these parameters are suitable for detailed MD simulations.

Graphical analyses of the complexes and figure generation were performed using UCSF Chimera[18] and the Molecular Operating Environment (MOE) package.[46]

ASSOCIATED CONTENT

Ⓢ Supporting Information

The Supporting Information is available free of charge on the ACS Publications website at DOI: 10.1021/jacs.9b00104.

Table S1 (comparison of backbone and glycosidic torsion angles in the native and PS2-modified RNA aptamer−thrombin complexes) (PDF)

Movie depicting the morphing between the native and PS2-modified RNA aptamer−thrombin complexes (MPG)

AUTHOR INFORMATION

Corresponding Authors

*martin.egli@vanderbilt.edu
*terry.p.lybrand@vanderbilt.edu

ORCID Ⓘ

Martin Egli: 0000-0003-4145-356X
Terry P. Lybrand: 0000-0002-2248-104X

Author Contributions

#M.E. and T.P.L. have contributed equally.

Notes

The authors declare no competing financial interest.

ACKNOWLEDGMENTS

REFERENCES

(1) Ng, E. W.; Shima, D. T.; Calias, P.; Cunningham, E. T., Jr.; Guyer, D. R.; Adamis, A. P. Pegaptanib, a targeted anti-VEGF aptamer for ocular vascular disease. *Nat. Rev. Drug Discovery* 2006, 5, 123.

(2) Bouchard, P. R.; Hutabarat, R. M.; Thompson, K. M. Discovery and development of therapeutic aptamers. *Annu. Rev. Pharmacol. Toxicol.* 2010, 50, 237.

(3) Keefe, A. D.; Pai, S.; Ellington, A. Aptamers as therapeutics. *Nat. Rev. Drug Discovery* 2010, 9, 537.

(4) Fang, X.; Tan, W. Aptamers generated from cell-SELEX for molecular medicine: a chemical biology approach. *Acc. Chem. Res.* 2010, 43, 48.

(5) Hamula, C. L. A.; Zhang, H.; Li, F.; Wang, Z.; Le, X. C.; Li, X.-F. Selection and analytical applications of aptamers binding microbial pathogens. *TrAC, Trends Anal. Chem.* 2011, 30, 1587.

(6) McKeague, M.; Derosa, M. C. Challenges and opportunities for small molecule aptamer development. *J. Nucleic Acids* 2012, 2012, 1.

(7) Germer, K.; Leonard, M.; Zhang, X. RNA aptamers and their therapeutic and diagnostic applications. *Int. J. Biochem. Mol. Biol.* 2013, 4, 27.

(8) Zhou, W.; Huang, P. J.; Liu, J. Aptamer-based biosensors for biomedical diagnostics. *Analyst* 2014, 139, 2627.

(9) Deng, B.; Lin, Y.; Wang, C.; Li, F.; Wang, Z.; Zhang, H.; Li, X.-F.; Le, X. C. Aptamer binding assays for proteins: the thrombin example - a review. *Anal. Chim. Acta* 2014, 837, 1.

(10) Xiang, D.; Shigdar, S.; Qiao, G.; Wang, T.; Kouzani, A. Z.; Zhou, S.-F.; Kong, L.; Li, Y.; Pu, C.; Duan, W. Nucleic acid aptamer-guided cancer therapeutics and diagnostics: the next generation of cancer medicine. *Theranostics* 2015, 5, 23.

(11) Nimjee, S. M.; White, R. R.; Becker, R. C.; Sullenger, B. A. Aptamers as therapeutics. *Annu. Rev. Pharmacol. Toxicol.* 2017, 57, 61.

(12) Ruckman, J.; Green, L. S.; Beeson, J.; Waugh, S.; Gillette, W. L.; Henninger, D. D.; Claesson-Welsh, L.; Janjic, N. 2'-Fluoropyrimidine RNA-based aptamers to the 165-amino acid form of vascular endothelial growth factor (VEGF165). Inhibition of receptor binding and VEGF-induced vascular permeability through interactions requiring the exon 7-encoded domain. *J. Biol. Chem.* 1998, 273, 20556.

(13) Burmeister, P. E.; Lewis, S. D.; Silva, R. F.; Preiss, J. R.; Horwitz, L. R.; Pendergrast, P. S.; McCauley, T. G.; Kurz, J. C.; Epstein, D. M.; Wilson, C.; Keefe, A. D. Direct in vitro selection of a 2'-O-methyl aptamer to VEGF. *Chem. Biol.* 2005, 12, 25.

(14) Gupta, S.; Hirota, M.; Waugh, S. M.; Murakami, I.; Suzuki, T.; Muraguchi, M.; Shibamori, M.; Ishikawa, Y.; Jarvis, T. C.; Carter, J. D.; Zhang, C.; Gawande, B.; Vrkljan, M.; Janjic, N.; Schneider, D. J. Chemically modified DNA aptamers bind interleukin-6 with high affinity and inhibit signaling by blocking its interaction with interleukin-6 receptor. *J. Biol. Chem.* 2014, 289, 8706.

(15) Ferreira-Bravo, I. A.; Cozens, C.; Holliger, P.; DeStefano, J. J. Selection of 2'-deoxy-2'-fluororarabinonucleotide (FANA) aptamers that bind HIV-1 reverse transcriptase with picomolar affinity. *Nucleic Acids Res.* 2015, 43, 9587.

(16) Abeydeera, N. D.; Egli, M.; Cox, N.; Mercier, K.; Conde, J. N.; Pallan, P. S.; Mizurini, D. M.; Sierant, M.; Hibti, F.-E.; Hassell, T.; Wang, T.; Liu, F.-W.; Liu, H.-M.; Martinez, C.; Sood, A. K.; Lybrand, T. P.; Frydman, C.; Monteiro, R. Q.; Gomer, R. H.; Nawrot, B.; Yang, X. Evoking picomolar binding in RNA by a single phosphorodithioate linkage. *Nucleic Acids Res.* 2016, 44, 8052.

(17) Long, S. B.; Long, M. B.; White, R. R.; Sullenger, B. A. Crystal structure of an RNA aptamer bound to thrombin. *RNA* 2008, 14, 2504.

(18) Pettersen, E. F.; Goddard, T. D.; Huang, C. C.; Couch, G. S.; Greenblatt, D. M.; Meng, E. C.; Ferrin, T. E. UCSF Chimera — a visualization system for exploratory research and analysis. *J. Comput. Chem.* 2004, 25, 1605.

(19) Hartley, B. S.; Shotton, D. M. Pancreatic elastase. In *The Enzymes*, 3rd ed.; Boyer, P. D., Ed.; Academic Press: New York/London, 1971; Vol. 3, pp 323−373.

(20) Pallan, P. S.; Yang, X.; Sierant, M.; Dinuka Abeydeera, N.; Hassell, T.; Martinez, C.; Janicka, M.; Nawrot, B.; Egli, M. Crystal structure, stability and Ago2 affinity of phosphorodithioate-modified RNAs. *RSC Adv.* **2014**, *4*, 64901.

(21) Wu, S. Y.; Yang, X.; Gharpure, K. M.; Hatakeyama, H.; Egli, M.; McGuire, M. H.; Nagaraja, A. S.; Miyake, T. M.; Rupaimoole, R.; Pecot, C. V.; Taylor, M.; Pradeep, S.; Sierant, M.; Rodriguez-Aguayo, C.; Choi, H. J.; Previs, R. A.; Armaiz-Pena, G. N.; Huang, L.; Martinez, C.; Hassell, T.; Ivan, C.; Sehgal, V.; Singhania, R.; Han, H. D.; Su, C.; Kim, J. H.; Dalton, H. J.; Kovvali, C.; Keyomarsi, K.; McMillan, N. A. J.; Overwijk, W. W.; Liu, J.; Lee, J. S.; Baggerly, K. A.; Lopez-Berestein, G.; Ram, P. T.; Nawrot, B.; Sood, A. K. 2'-OMe-Phosphorodithioate-modified siRNAs show increased loading into the RISC complex and enhanced anti-tumour activity. *Nat. Commun.* **2014**, *5*, 3459.

(22) Ringer, A. L.; Senenko, A.; Sherrill, C. D. Models of S/π interactions in protein structures: comparison of the H_2S-benzene complex with PDB data. *Protein Sci.* **2007**, *16*, 2216.

(23) Yang, X.; Abeydeera, N. D.; Liu, F.-W.; Egli, M. Origins of the enhanced affinity of RNA−protein interactions triggered by RNA phosphorodithioate backbone modification. *Chem. Commun.* **2017**, *53*, 10508.

(24) Schirle, N. T.; Sheu-Gruttadauria, J.; MacRae, I. J. Structural basis for microRNA targeting. *Science* **2014**, *346*, 608−613.

(25) Zandarashvili, L.; Nguyen, D.; Anderson, K. M.; White, M. A.; Gorenstein, D. G.; Iwahara, J. Entropic enhancement of protein-DNA affinity by oxygen-to-sulfur substitution in DNA phosphate. *Biophys. J.* **2015**, *109*, 1026−1037.

(26) Khanarian, G.; Moore, W. J. The Kerr effect of amino acids in water. *Aust. J. Chem.* **1980**, *33*, 1727.

(27) McMeekin, T. L.; Wilensky, M.; Groves, M. L. Refractive indices of proteins in relation to amino acid composition and specific volumes. *Biochem. Biophys. Res. Commun.* **1962**, *7*, 151.

(28) Swart, M.; Snijders, J. G.; van Duvijnen, P. Th. Polarizabilities of amino acid residues. *J. Comput. Methods Sci. Eng.* **2004**, *4*, 419.

(29) Millefiori, S.; Alparone, A.; Millefiori, A.; Vanella, A. Electronic and vibrational polarizabilities of the twenty naturally occurring amino acids. *Biophys. Chem.* **2008**, *132*, 139.

(30) Antonijević, I. S.; Janjić, G. V.; Milčić, M. K.; Zarić, S. D. Preferred geometries and energies of sulfur-sulfur interactions in crystal structures. *Cryst. Growth Des.* **2016**, *16*, 632.

(31) Frisch, M. J.; Trucks, G. W.; Schlegel, H. B.; Scuseria, G. E.; Robb, M. A.; Cheeseman, J. R.; Scalmani, G.; Barone, V.; Petersson, G. A.; Nakatsuji, H.; Li, X.; Caricato, M.; Marenich, A.; Bloino, J.; Janesko, B. G.; Gomperts, R.; Mennucci, B.; Hratchian, H. P.; Ortiz, J. V.; Izmaylov, A. F.; Sonnenberg, J. L.; Williams-Young, D.; Ding, F.; Lipparini, F.; Egidi, F.; Goings, J.; Peng, B.; Petrone, A.; Henderson, T.; Ranasinghe, D.; Zakrzewski, V. G.; Gao, J.; Rega, N.; Zheng, G.; Liang, W.; Hada, M.; Ehara, M.; Toyota, K.; Fukuda, R.; Hasegawa, J.; Ishida, M.; Nakajima, T.; Honda, Y.; Kitao, O.; Nakai, H.; Vreven, T.; Throssell, K.; Montgomery, J. A., Jr.; Peralta, J. E.; Ogliaro, F.; Bearpark, M.; Heyd, J. J.; Brothers, E.; Kudin, K. N.; Staroverov, V. N.; Keith, T.; Kobayashi, R.; Normand, J.; Raghavachari, K.; Rendell, A.; Burant, J. C.; Iyengar, S. S.; Tomasi, J.; Cossi, M.; Millam, J. M.; Klene, M.; Adamo, C.; Cammi, R.; Ochterski, J. W.; Martin, R. L.; Morokuma, K.; Farkas, O.; Foresman, J. B.; Fox, D. J. *Gaussian 09*, revision D.01; Gaussian, Inc.: Wallingford, CT, 2009.

(32) Su, P.; Li, H. Energy decomposition analysis of covalent bonds and intermolecular interactions. *J. Chem. Phys.* **2009**, *131*, No. 014102.

(33) Schmidt, M. W.; Baldridge, K. K.; Boatz, J. A.; Elbert, S. T.; Gordon, M. S.; Jensen, J. H.; Koseki, S.; Matsunaga, N.; Nguyen, K. A.; Su, S.; Windus, T. L.; Dupuis, M.; Montgomery, J. A. General atomic and molecular electronic structure system. *J. Comput. Chem.* **1993**, *14*, 1347.

(34) Miertus, S.; Scrocco, E.; Tomasi, J. Electrostatic interaction of a solute with a continuum. A direct utilization of ab initio molecular potentials for the prevision of solvent effects. *Chem. Phys.* **1981**, *55*, 117.

(35) Marenich, A. V.; Cramer, C. J.; Truhlar, D. G. Universal solvation model based on solute electron density and on a continuum model of the solvent defined by the bulk dielectric constant and atomic surface tensions. *J. Phys. Chem. B* **2009**, *113*, 6378.

(36) Case, D. A.; Babin, V.; Berryman, J. T.; Betz, R. M.; Cai, Q.; Cerutti, D. S.; Cheatham, T. E., III; Darden, T. A.; Duke, R. E.; Gohlke, H.; Goetz, A. W.; Gusarov, S.; Homeyer, N.; Janowski, P.; Kaus, J.; Kolossváry, I.; Kovalenko, A.; Lee, T. S.; LeGrand, S.; Luchko, T.; Luo, R.; Madej, B.; Merz, K. M.; Paesani, F.; Roe, D. R.; Roitberg, A.; Sagui, C.; Salomon-Ferrer, R.; Seabra, G.; Simmerling, C. L.; Smith, W.; Swails, J.; Walker, R. C.; Wang, J.; Wolf, R. M.; Wu, X.; Kollman, P. A. *AMBER14*; University of California: San Francisco, CA, 2014.

(37) Maier, J. A.; Martinez, C.; Kasavajhala, K.; Wickstrom, L.; Hauser, K. E.; Simmerling, C. ff14SB: Improving the accuracy of protein side chain and backbone parameters from ff99SB. *J. Chem. Theory Comput.* **2015**, *11*, 3696.

(38) Berendsen, H. J. C.; Grigera, J. R.; Straatsma, T. P. The missing term in effective pair potentials. *J. Phys. Chem.* **1987**, *91*, 6269.

(39) Joung, I. S.; Cheatham, T. E., III. Determination of alkali and halide monovalent ion parameters for use in explicitly solvated biomolecular simulations. *J. Phys. Chem. B* **2008**, *112*, 9020.

(40) Li, P.; Song, L.; Merz, K., Jr. Parameterization of highly charged metal ions using the 12−6-4 LJ-type nonbonded model in explicit water. *J. Phys. Chem. B* **2015**, *119*, 883.

(41) Cerutti, D. S.; Duke, R. E.; Darden, T. A.; Lybrand, T. P. Staggered Mesh Ewald: an extension of the Smooth Particle-Mesh Ewald method adding great versatility. *J. Chem. Theory Comput.* **2009**, *5*, 2322.

(42) Izaguirre, J. A.; Catarello, D. P.; Wozniak, J. M.; Skeel, R. D. Langevin stabilization of molecular dynamics. *J. Chem. Phys.* **2001**, *114*, 2090.

(43) Ryckaert, J. P.; Ciccotti, G.; Berendsen, H. J. C.; Hirasawa, K. Numerical integration of the cartesian equations of motion of a system with constraints: molecular dynamics of n-alkanes. *J. Comput. Phys.* **1977**, *23*, 327.

(44) Miyamoto, S.; Kollman, P. A. Settle: An analytical version of the SHAKE and RATTLE algorithm for rigid water models. *J. Comput. Chem.* **1992**, *13*, 952.

(45) Bayly, C.; Cieplak, P.; Cornell, W.; Kollman, P. A well-behaved electrostatic potential based method using charge restraints for deriving atomic charges: the RESP model. *J. Phys. Chem.* **1993**, *97*, 10269.

(46) *Molecular Operating Environment (MOE)*, 2018.0101; Chemical Computing Group, Inc., Montreal, Canada, 2018.